Pure & Appl. Chem., Vol. 57, No. 11, pp. 1603–1616, 1985.
Printed in Great Britain.

Characterization of molecular order in solid polymers by rheo-optical Fourier-transform infrared spectroscopy: recent advances

H. W. Siesler

Bayer AG, Werk Dormagen, Research & Development, D 4047 Dormagen, FRG

Abstract - In the late seventies rheo-optical Fourier-Transform infrared (FTIR) spectroscopy has emerged as an extremely valuable tool to study deformation and relaxation phenomena on-line to the mechanical treatment of polymeric solids. The present contribution is intended to demonstrate the potential of the technique with reference to recent experimental results of selected thermoplastic and elastomeric polymer systems.

INTRODUCTION

The increased need for more detailed experimental data and a better understanding of the molecular mechanisms involved in polymer deformation and relaxation has led to the search for new experimental techniques for the characterization of transient structural changes during mechanical processes. Primarily the rapid-scanning capability of the FTIR technique offered the possibility to combine vibrational spectroscopy with mechanical measurements in analogy to other rheo-optical methods (ref. 1). Basically, in rheo-optics a mechanical test is combined with one of various types of optical measurements (e.g. birefringence, light scattering, x-ray diffraction or infrared absorption) and the relation between stress, strain and the simultaneously measured optical quantity is established (refs. 2-4). Thus, spectroscopic parameters of the conformation, crystallization (intensity of conformation- and crystallization-sensitive absorption bands) and orientation (dichroism of absorption bands belonging to different phases or domains) can be monitored on-line to the deformation, recovery or stress-relaxation of the polymer under examination in very small strain or time intervals relative to the total elongation or time scale of the mechanical process.

EXPERIMENTAL AND SOFTWARE

The experimental principles of rheo-optical FTIR spectroscopy are illustrated in Fig. 1. The interferograms which are subsequently transformed to the corresponding spectra were obtained on a Nicolet 7199 FTIR spectrometer equipped with a Nicolet 1280 computer. The electromechanical apparatus and the polarizer unit constructed for the simultaneous measurement of FTIR

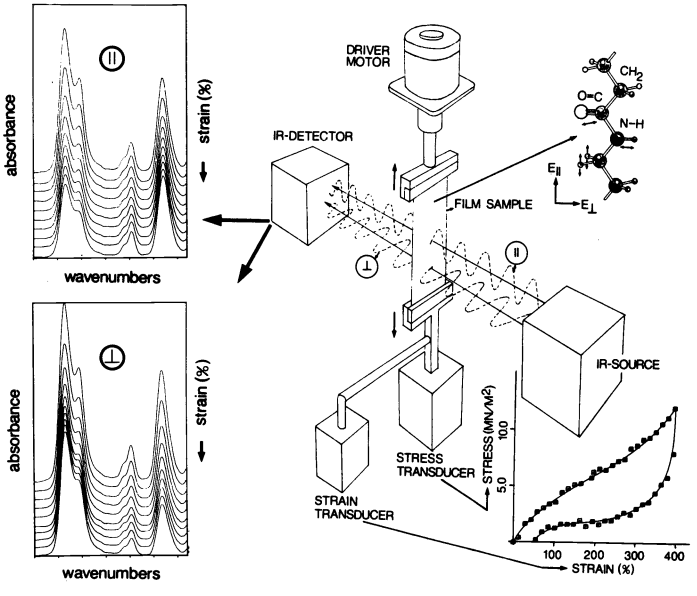

Fig. 1 Experimental scheme of rheo-optical FTIR spectroscopy of polymers.

polarization spectra and stress-strain diagrams during elongation and stress-relaxation of polymer films at variable temperature have been described in detail elsewhere (ref. 1). Basically, the stretching machine is mounted on a x-y-stage in the sample compartment of the spectrometer and the specimen to be tested is held between two clamps which are attached to force and displacement transducers, respectively, and can be uniaxially drawn at variable elongation rates. Apart from the on-line plot of the two mechanical quantities their corresponding voltages at the stress and strain gauges are digitally converted and stored in the data file of the previously scanned interferogram. Taking into account the original sample geometry these data can finally be utilized for the graphical representation of the stress-strain diagram of the polymer under investigation (Fig. 1). For orientation measurements the polarization direction of the incident radiation is alternately adjusted parallel and perpendicular to the stretching direction at the end of each scan by a pneumatically rotatable polarizer unit which is also controlled by the computer of the FTIR system.

For the routine analysis of the spectra series acquired during the rheo-optical experiment the automated information processing capability of the system is exploited with the aid of a specifically developed BASIC software and programs are applied which are based on the evaluation of the integral or peak-maximum intensity (with or without automatic peak search) and automatically calculate the following spectroscopic parameters:

1. the dichroic ratio R (refs. 1,5-7):

$$R = A_{\parallel}/A_{\perp} \tag{1}$$

2. the structural absorbance A_o (refs. 1,5-7):

$$A_o = (A_{\parallel} + 2A_{\perp})/3 \tag{2}$$

3. the dichroic function DF (ref. 8):

$$DF = (R - 1)/(R + 2) \tag{3}$$

4. in the case of well-defined transition moment directions the frequently used orientation function f (refs. 1,5-8). Thus, for an absorption band having its transition moment parallel or perpendicular to the chain axis f reads:

$$f_{\parallel} = (R - 1)/(R + 2) \tag{4a}$$

and

$$f_{\perp} = -2\cdot(R - 1)/(R + 2) \tag{4b}$$

For a detailed discussion of the theory of orientational measurements in polymers using infrared dichroism the reader is referred to the pertinent literature (refs. 5-7). The values of the abovementioned parameters for specified absorption bands of the individual spectra were determined by appropriately correlating the absorbance values $A_{\parallel}$ and $A_{\perp}$ successively measured with light polarized parallel and perpendicular, respectively, to the stretching direction. The structural absorbance has been chosen as intensity parameter because it eliminates the influence of changing orientation on the actual intensity of an absorption band. Changes in sample thickness during elongation were compensated by comparing against a suitable reference band. The representation of the orientation data in terms of the dichroic function was chosen because of its proportionality to the frequently used orientation function (ref. 8) despite the lack of knowledge of the exact transition moment directions of the investigated absorption bands. Upon data processing the individual spectroscopic parameters can be plotted as a function of strain or time in an operator-selected format with a separate software routine.

EXPERIMENTAL RESULTS

Stretching-induced II(α)-I(β) crystal phase transformation in poly(vinylidene fluoride)

Poly(vinylidene fluoride) (PVF_2) is a polymer with exceptional technological and scientific properties. Depending upon the thermal, mechanical and electrical pretreatment the polymer can exist in four different modifications denoted I(β), II(α), III(γ) and $IV_p(\delta)$ or $IV_p(\alpha_p)$. The crystal system of the forms I(β) and II(α) is orthorhombic and their molecular conformations are TT and $TGT\bar{G}$, respectively. Form III(γ) belongs to the monoclinic system with a $T_3GT_3\bar{G}$ conformation. Form $IV_p(\delta)$ is formed by poling the II(α) form at high electric fields. The two polymorphs have the same chain conformation and unit-cell dimensions and differ only in the interchain packing. The crystal structures of the different forms, the conditions of their formation and mutual transformation by tensile force, high pressure, heat treatment or electrical fields have been reported in detail by several authors (refs. 9-13). Although a number of infrared and Raman studies have been done on the various phases of PVF_2 (refs. 14,15) no data on dynamic investigations are so far available. In view of the well-established band assignments and the significant differences in the IR spectra of the II(α) and I(β) modifications the rheo-optical FTIR technique has proved particularly suitable to study the conforma-

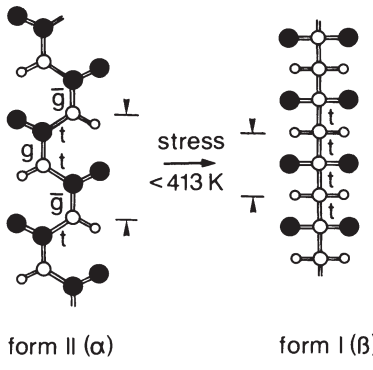

Fig. 2 Conformational changes of the stretching-induced II(α)-I(β) crystal transformation in PVF_2.

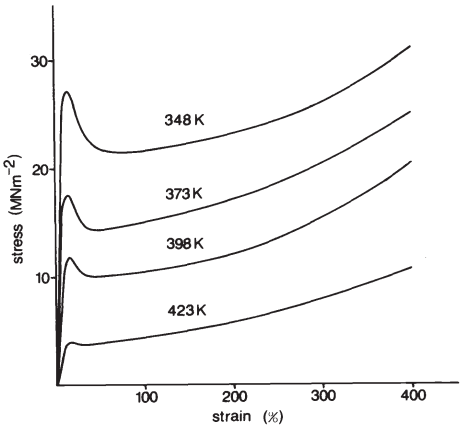

Fig. 3 Stress-strain diagrams of unoriented PVF_2 films in the II(α) modification at different temperatures.

tional changes from the TGTḠ to the all-trans form in the II(α)-I(β) crystal transformation (Fig. 2) on-line to the drawing procedure as a function of temperature (ref. 16).

In the mechanical treatment PVF_2 film specimens in the unoriented II(α) modification were subjected to uniaxial elongation upto 400% strain with an elongation rate of 95%/minute at 348 K, 373 K, 398 K and 423 K and 1O-scan FTIR polarization spectra were taken with light alternately polarized parallel and perpendicular to the direction of stretch in 5-second intervals at a resolution of 4 cm^{-1}. The films had been prepared from PVF_2 granulate by hot-pressing at 483 K and melt crystallization at room temperature and had a density of 1.782 gcm^{-3} as measured in a carbontetrachloride/ethylenbromide mixture. From these specimens film strips with a thickness between 0.030 and 0.035 mm and gauge dimensions of 8 x 4 mm were prepared for the rheo-optical FTIR investigations. The wide-angle x-ray diffraction photographs were taken on a Kiessig flat-camera with Ni-filtered Cu-K_α radiation.

The stress-strain diagrams of the individual experiments at different temperatures are shown in Fig. 3. Apart from the drastic reduction of the stress level with increasing temperature the most obvious feature is the almost complete disappearance of the stress-decreasing region beyond the yield point. Nevertheless, neck formation was observed throughout the investigated temperature interval and its propagation over the total sample area was generally completed below 400% strain. Previous rheo-optical wide-angle x-ray measurements (ref. 11) had also revealed that this II(α)-I(β) crystal transformation occurred below 413 K with the sample deforming by formation of a neck whereas above this temperature no changes in crystal modification were observed. Due to the lower elongation rate of 5% strain/minute, however, these authors observed that at temperatures above 413 K the samples were found to deform uniformly without necking.

Wide-angle x-ray diffraction photographs taken at room temperature of the undrawn film specimen and of the samples drawn at different temperatures upto 400% strain in the stress-relaxed state are shown in Fig. 4. The intensities of the combined (100)/(020) and (110) reflections of modification II(α) at about $2\theta = 18^o$ and 20^o, respectively, and the combined (200)/(110) reflections of modification I(β) at about $2\theta = 21^o$ clearly reflect the decreasing proportion of crystals transformed to the I(β) modification with increasing temperature (refs. 11,12). Specific wavenumber regions of the polarization spectra taken at 348 K as a function of strain are shown in Fig. 5. With increasing elongation the spectra series are characterized by the

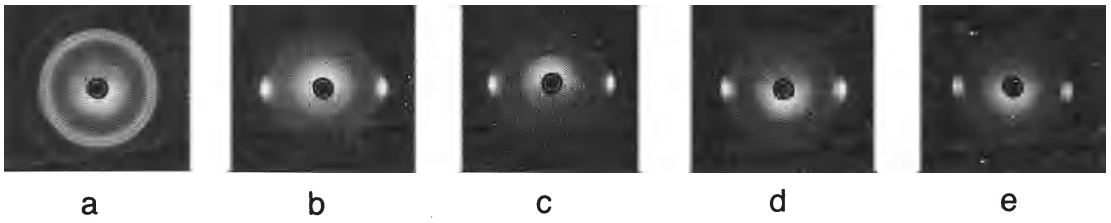

Fig. 4 Wide-angle x-ray diagrams of the original PVF_2 film in the unoriented II(α) modification (a) and of the stress-relaxed samples elongated to 400% strain at 348 K (b), 373 K (c), 398 K (d) and 423 K (e).

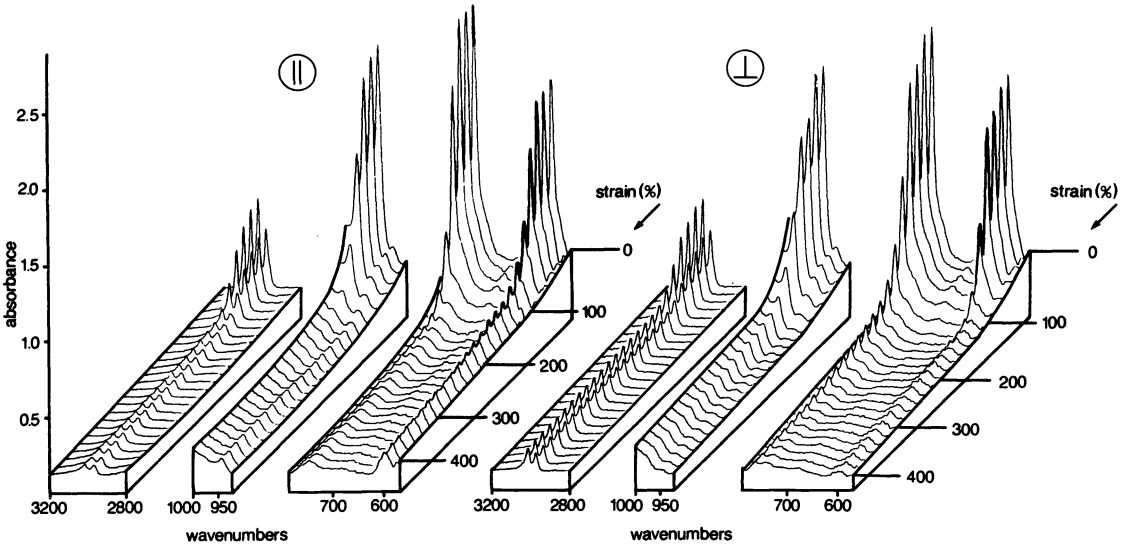

Fig. 5 FTIR polarization spectra taken during elongation at 348 K of a PVF_2 film with an initial II(α) crystal structure.

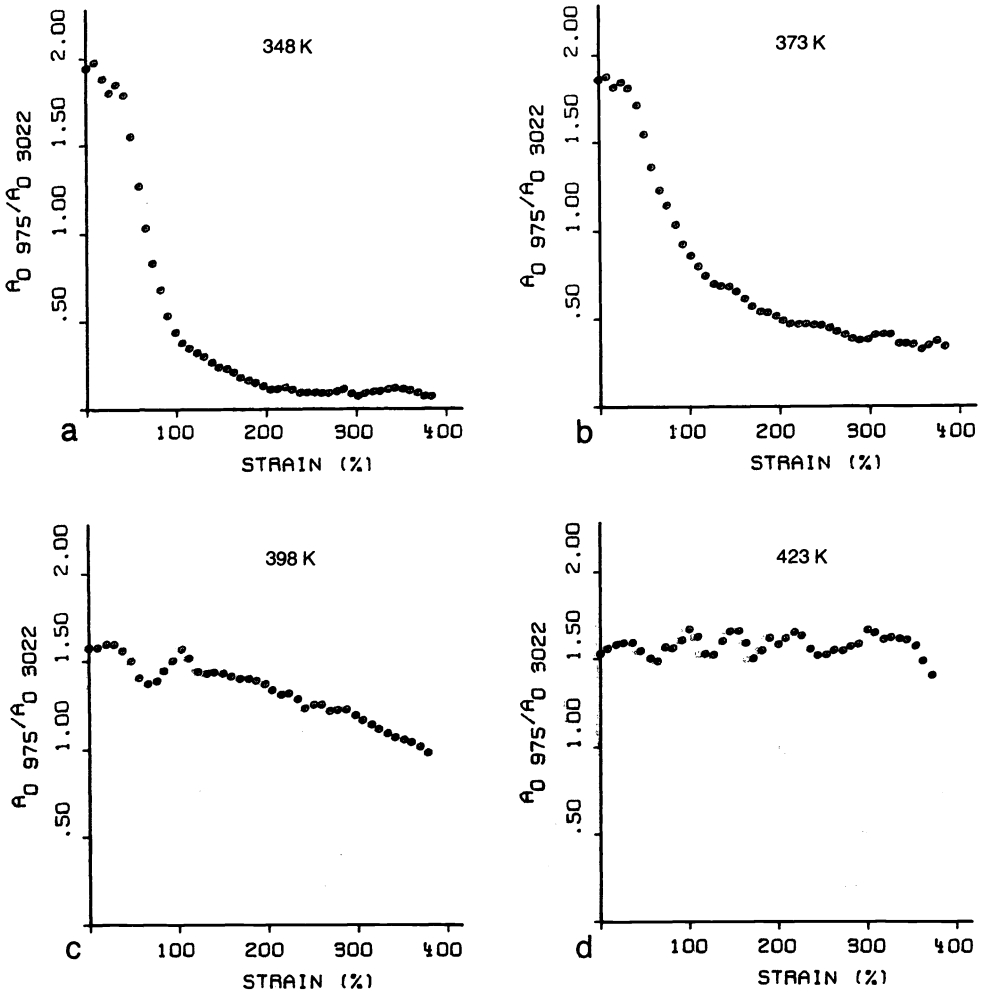

Fig. 6 Variations of the structural absorbance ratio A_{o975}/A_{o3022} as a function of strain at different temperatures: (a) 348 K, (b) 373 K, (c) 398 K and (d) 423 K.

disappearance of those absorption bands which are assigned to the TGTG conformation of the II(α) modification and clearly indicate the complete transformation into the all-trans I(β) form at this temperature. This result is also supported by the absence of the (100)/(020) and (110) reflections of the II(α) modification in the wide-angle x-ray diagram of Fig. 4b. For the detailed representation of the modificational changes during uniaxial elongation at different temperatures the structural absorbance of the 975 cm^{-1} absorption band of the II(α) form has been ratioed against the structural absorbance of the $\nu_a(CH_2)$ absorption at 3022 cm^{-1} as a suitable thickness reference band and plotted in dependence of strain in Figs. 6a-d. While regions with a drastic drop in the intensity ratio are observable at 348 K and 373 K a more or less linear decrease occurs at 398 K and no significant changes take place at 423 K. Thus, assuming that according to the FTIR measurements at 348 K form II(α) has been completely transformed to modification I(β) upon elongation to 400% strain, approximately 15% of phase II(α) have been retained at 373 K. Furthermore, a proportion of about 58% of form II(α) has resisted the mechanical treatment upto 400% strain at 398 K and deformation at 423 K only leads to an orientation of modification II(α) with no significant transformation into form I(β).

To demonstrate that neck-formation takes place throughout the investigated temperature interval separate experiments upto 100% elongation only have been performed at 348 K and 423 K. Thus, it could be shown (ref. 16) that at 100% strain the sample drawn at 348 K consists of a neck region which according to wide-angle x-ray diffraction and IR spectroscopy has been transformed to a large degree into the I(β) form and a thicker, unoriented region which is almost completely retained in the II(α) modification. The sample drawn at 423 K upto 100% strain can also be separated macroscopically into two regions with the difference, however, that both regions contain modification II(α) only, in the unoriented and highly oriented state, respectively. The steep decrease of the A_{o975}/A_{o3022} intensity ratio observed between 50 and 100% strain at 348 K and 373 K is therefore a consequence of the propagation of the neck past the sampling area in the IR beam. Hence, the initiation of the crystal transformation is primarily based on a heterogeneous stress-distribution during neck formation whose decreasing influence with increasing temperature is reflected in the enhancement of the proportion of retained II(α) form.

Strain-induced crystallization of sulfur-crosslinked natural rubber

Apart from the degree of crosslinking the mechanical properties of a polymer having network structure are strongly influenced by strain-induced crystallization (refs. 17-23). This phenomenon is of great practical importance both during processing (ref. 21) and with regard to the technological properties of the product such as tear strength and maximum extensibility (ref. 22). A schematic representation of strain-induced crystallization within a polymer network which has been elongated by a force in the specified direction is shown in Fig. 7.

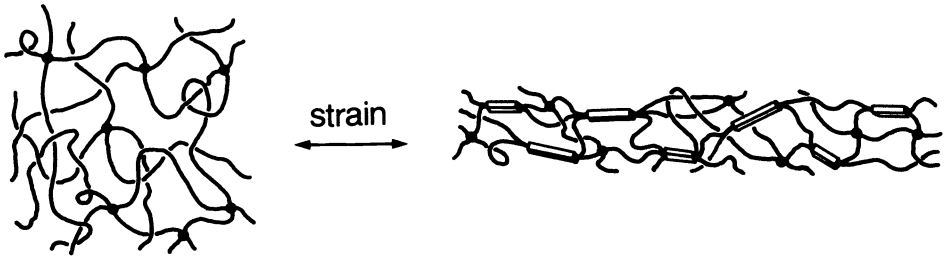

Fig. 7 Schematic representation of strain-induced crystallization in a crosslinked elastomer.

Crystallites thus formed act as crosslinks of high functionality and since they are nondeformable at the stress levels involved, diminish the amount of elastomeric material able to respond to the imposed stress. Additionally, these crystallites act as filler particles which generally increase the modulus of a rubber-like material (ref. 22). In the stress-strain diagram strain-induced crystallization affects a drastic increase of elastic force with strain as a consequence of a significant selfreinforcement of the elastomer during elongation (refs. 17-22). In this context rheo-optical FTIR spectroscopy has proved a valuable technique to study strain-induced crystallization on-line to the deformation process of the elastomer under examination. Thus, the onset and progress of strain-induced crystallization during elongation and its disappearance upon recovery can be readily monitored simultaneously to the stress-strain measurements by the intensity of an absorption band which is characteristic of the threedimensional order in the crystalline phase.

In the mechanical treatment the sulfur-crosslinked (1.8% S) natural rubber (100% 1,4-cis-polyisoprene) film sample with gauge dimensions 10 x 4 mm and a thickness of approximately 0.100 mm was subjected to three successive loading-unloading cycles upto 545, 545 and 650% strain, respectively, with an elongation and recovery rate of 85% strain/minute and 15-scan

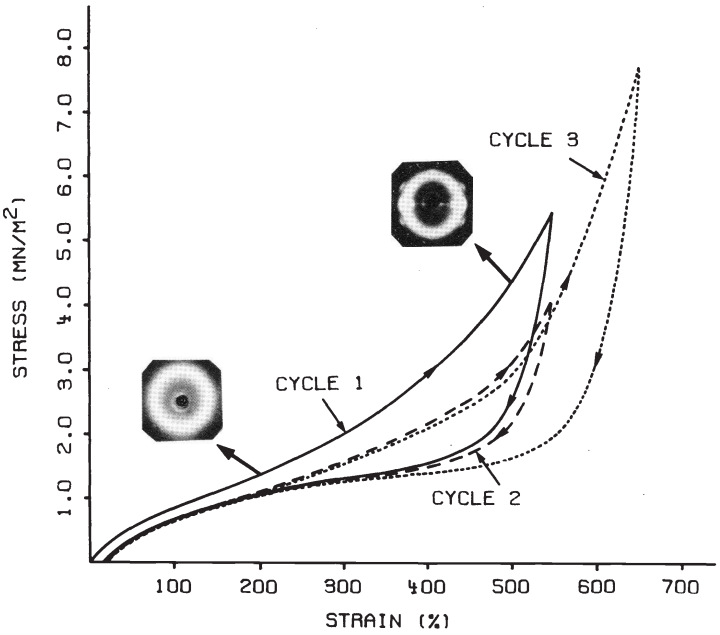

Fig. 8 Stress-strain diagram of three successive loading-unloading cycles of a sulfur-crosslinked natural rubber film at 300 K.

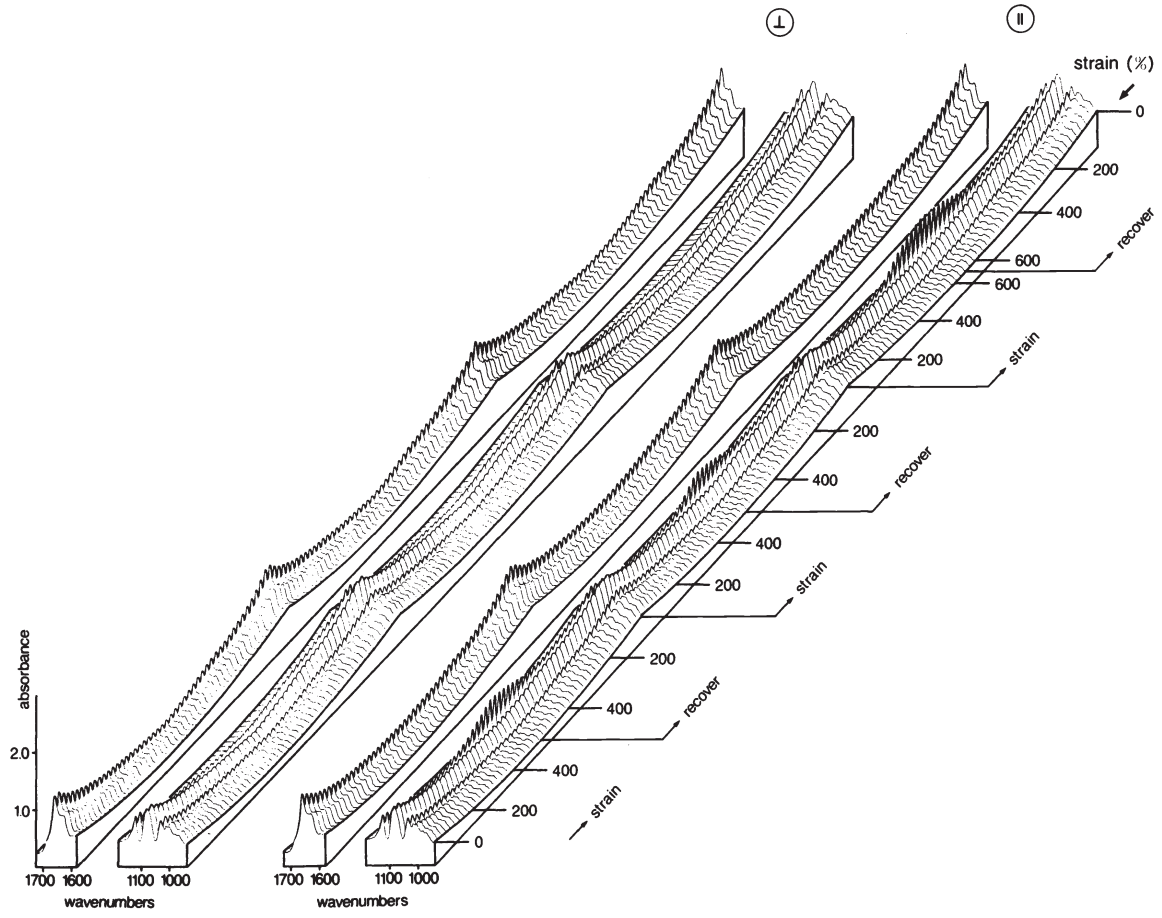

Fig. 9 FTIR polarization spectra in the ν(C=C) and C-CH_3 in-plane bending region taken during the mechanical treatment outlined in Fig. 8.

spectra were taken with light alternately polarized parallel and perpendicular to the direction of stretch at 300 K in 8-second intervals with a resolution of 4 cm^{-1}. The total number of FTIR spectra acquired simultaneously to the three loading-unloading cycles was 300. The stress-strain diagram corresponding to the mechanical treatment is shown in Fig. 8. In the first cycle the wide-angle x-ray diagrams taken at 200% and 500% strain, respectively, of the stress-relaxed samples have been included to demonstrate the improvement of the state of order during elongation. The stress-hysteresis arises from the tendency of the crystals formed on extension to persist as the tensile force is reduced. Ultimately, however, the amorphous state is recovered and the stress approaches the corresponding values of the loading half-cycle. Generally, a significant reduction of the stress-hysteresis and the maximum stress level can be observed upon reelongation to the maximum strain value of the virgin cycle (see Fig. 8, cycles 1 and 2). The polarization spectra monitored during the elongation-recovery cycles are shown separately for the two polarization directions in Fig. 9. Based upon a previous absorbance subtraction procedure (ref. 24) the 1126 cm^{-1} crystallinity-sensitive absorption band which has been assigned to a $C-CH_3$ in-plane deformation vibration (ref. 25) was used in conjunction with the $\nu(C=C)$ absorption band at 1662 cm^{-1} which is representative of the average polymer as thickness reference band to monitor the onset, progress and disappearance of strain-induced crystallization during the mechanical treatment. Thus, the ratio of the structural absorbances of the 1126 cm^{-1} and 1662 cm^{-1} bands was evaluated with the above-mentioned software routine for the individual spectra taken during the loading-unloading cycles and plotted as a function of strain in Fig. 10. These data clearly demonstrate the reversible nature of strain-induced crystallization and allow to assign a strain value of about 230% to the onset of crystallization in the first cycle. For an exact quantitative interpretation of the spectroscopic data the degree of crystallinity had to be determined by an independent method. In this respect detailed rheo-optical wide-angle x-ray investigations by synchrotron radiation are presently in progress. However, from comparative experiments of a non-crystallizing natural rubber system a value of the order of 10% could be derived as a rough approximation for the degree of crystallinity at 500% strain. Additionally, a significant retention of the strain-induced crystallinity relative to the loading half-cycle is observable during recovery. The maximum extent of crystallization clearly correlates with the maximum stress level of the corresponding loading-unloading cycle. Thus, a further increase of the maximum degree of crystallinity relative to the preceding cycle can be expected only, when the maximum elongation of a loading-unloading cycle exceeds the maximum elongation of the preceding cycle (see Figs. 8 and 10, cycles 2 and 3). A so far unreported effect becomes evident when the structural absorbance of the $\nu(C=C)$ thickness reference band is plotted as a function of strain (Fig. 11). Thus, dependent upon the degree of strain-induced crystallization a distinct asymmetry in the recovery of the original sample geometry could be detected. The phenomenon may be correlated with the composite nature of such a strain-crystallized system and must be interpreted in terms of a preferential recovery of the thickness relative to the transverse dimension in the stress-strain plateau region of the unloading half-cycle between 400 and 200% strain. To represent the orientation of the crystalline phase and the average polymer the dichroic functions of the 1126 cm^{-1} and 1662 cm^{-1} bands, respectively, have been plotted versus strain in Fig. 12. Here too, the maximum orientation taken up by the average polymer and the polymer chains in the crystalline regions correlates with the maximum

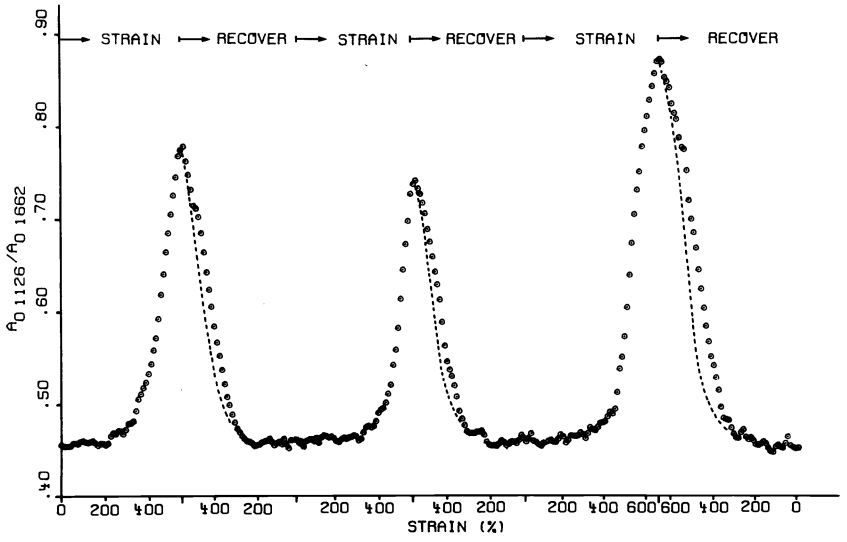

Fig. 10 Plot of the A_{o1126}/A_{o1662} structural absorbance ratio as a function of strain for the three successive loading-unloading cycles shown in Fig. 8.

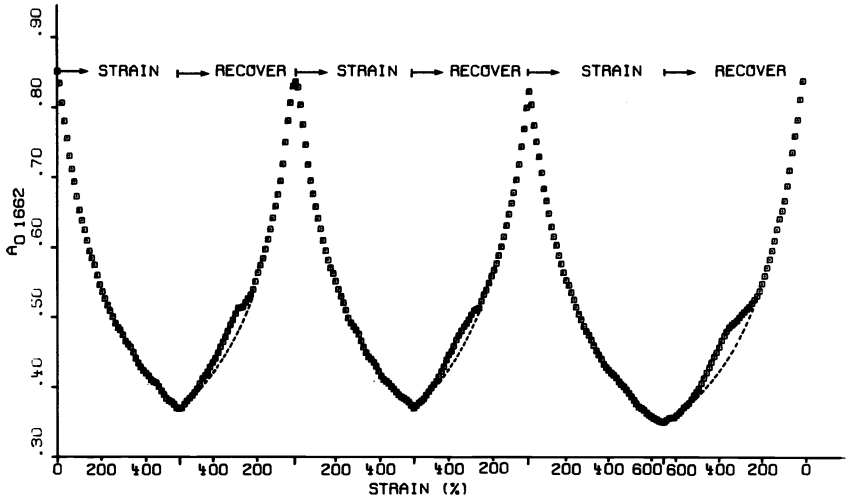

Fig. 11 Structural absorbance/strain-plot of the 1662 cm^{-1} thickness reference band of sulfur-crosslinked natural rubber.

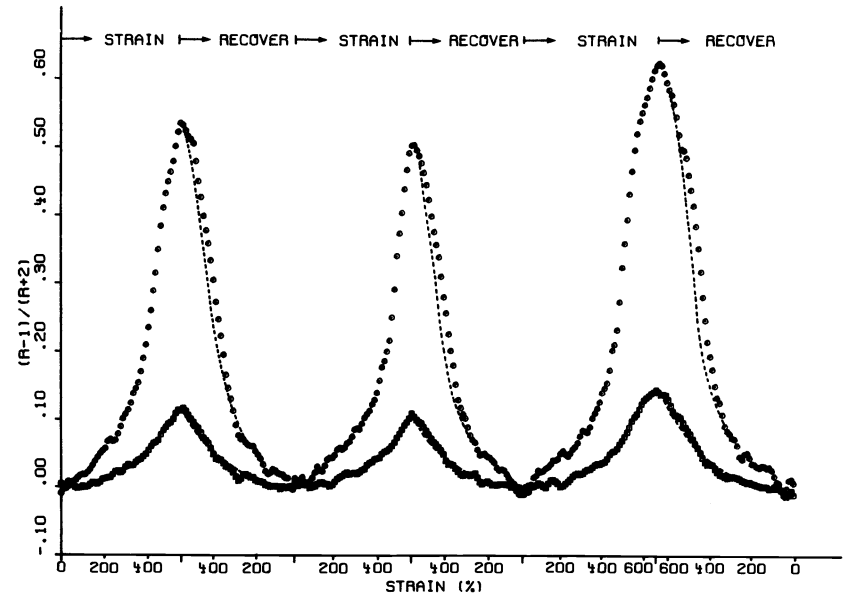

Fig. 12 Dichroic function/strain-plot of the 1126 cm^{-1} (⊙) and 1662 cm^{-1} (⊡) absorption bands for the mechanical treatment outlined in Fig. 8.

stress level of the corresponding elongation-recovery cycle. Additionally, the enhancement of chain alignment in the strain-crystallizing relative to the amorphous phase and the retention of crystallization upon unloading are readily detected. With reference to a previous detailed orientation analysis (ref. 24) it can be shown that based upon the assumption of a zero transition moment angle for the 1126 cm^{-1} band (the dichroic function is then equivalent to the orientation function of this absorption band) average inclination angles of approximately 40° and 30° are calculated for the average polymer and the polymer chains in the crystal phase, respectively, and the direction of stretch in the 650% drawn sample.

In separate experiments the influence of stress-relaxation on strain-induced crystallization and chain orientation in sulfur-crosslinked natural rubber was investigated by monitoring the 1126 cm^{-1} and 1662 cm^{-1} absorption intensities as a function of relaxation time at various stress levels (ref. 1). Interestingly, these measurements revealed, that crystallinity as well as crystalline and amorphous orientation further increased during the fast decay region of stress relaxation despite constant elongation. Taking into account the low degree of strain-induced crystallinity (see above) the observed stress relaxation can therefore be primarily ascribed to the amorphous phase.

Phase separation and segmental orientation in polyurethanes

The rheo-optical FTIR technique has also been applied to study segmental orientation in polyurethane films during uniaxial elongation and recovery (ref. 26). In fact, polyurethanes are particularly suited to such investigations because they contain functional groups with characteristic IR absorptions which can be assigned to specific domain locations of the polymer. Additional information may be obtained from measurements at elevated temperature and investigations of NH-deuterated samples because the isotope exchange offers a means to differentiate the hard segments into larger, phase-separated species and smaller, fibrillar units dispersed in the soft segments.

Linear polyurethanes are generally prepared by condensation of a diisocyanate with a macroglycol (commonly a polyether or polyester with a molecular weight between 1000 and 2000) and a low-molecular weight chain extender dialcohol or diamine. To demonstrate some of the characteristic features of segmental orientation in polyurethanes the rheo-optical FTIR technique is here demonstrated with reference to a series of polyester urethanes synthesized from diphenylmethan-4,4'-diisocyanate, a polyester based on adipic acid/butane diol/ethylene glycol (MW 2000) and butane diol with polyester : diisocyanate : chain extender molar ratios of 1.0 : 3.4 : 2.2 (a), 1.0 : 6.6 : 5.4 (b) and 1.0 : 8.7 : 7.5 (c). The soft segments of this type of polyurethane basically consist of the reaction products of the diisocyanate component and the macroglycol, whereas the hard segments contain largely aromatic and butane diol moieties linked together by urethane groups.

The segmental structure of polyurethanes becomes apparent from Fig. 13 which shows the linear

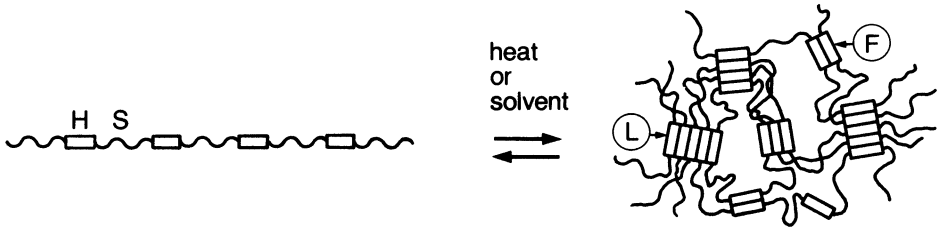

Fig. 13 Simplified scheme of phase separation in a polyurethane elastomer; H: hard segments, S: soft segments, F: fibrillar hard segments, L: lamellar hard segments.

polymer primary chains made up of alternating hard and soft segments. However, in the solid polymer the polymer chains do not really exist separately but rather the hard segments tend to associate with each other through hydrogen bonding and aromatic π-electron attraction. As a consequence, the hard segments form domains in the mobile soft segment matrix and a two-phase system with different types of hard segment morphology results:

fibrillar hard segments, where the long axis of the domains coincides with the polymer chain axes (Fig. 13 F) and

lamellar hard segments with their long axis direction perpendicular to the polymer chain axes (Fig. 13 L).

The separate hard segment domains crosslink the linear polymer primary chains and produce a network which accounts for the elastic character of the polymer. Generally, phase segregation plays an important role in the characterization and use of these polymers and numerous studies are available on their segmental structure, particularly the hard segment domains (refs. 27-33).

Film samples of the polyester urethanes under examination were prepared under identical conditions with a thickness of approximately 0.010 mm by casting from 2% (w/v) dimethylformamide solutions on surface-roughened glass plates and drying at 323 K in vacuum for 6 hours. The film samples were then peeled off the glass plates in hot water, treated with boiling water for 0.5 h (to remove residual solvent traces) and finally dried in vacuum at 323 K for 0.5 h. In the mechanical treatment film specimens with gauge dimensions 12 x 6 mm were subjected to a loading-unloading cycle upto 220% strain with an elongation and recovery rate of 72% strain/minute and 12-scan spectra were taken in 14-second intervals at a resolution of 2 cm^{-1}. Partially NH-deuterated specimens were prepared in a special deuteration cell (ref. 7) over a period of 5 days and finally transferred to the sample chamber of the stretching machine. The rheo-optical experiments were performed at 300 K and 348 K for the original samples and at 300 K for the partially NH-deuterated polymers.

The IR spectrum of one of the investigated polyester urethanes (b) is shown in Fig. 14. On the basis of the established frequency correlations for the functional groups of polyurethanes (ref. 27) the extent of soft and hard segment orientation can be monitored by means of the polarization properties of the $\nu(CH_2)$ (2959 cm^{-1}), $\nu(C{=}O)_{ester}$ (1733 cm^{-1}) and $\nu(NH)$ (3331 cm^{-1}),

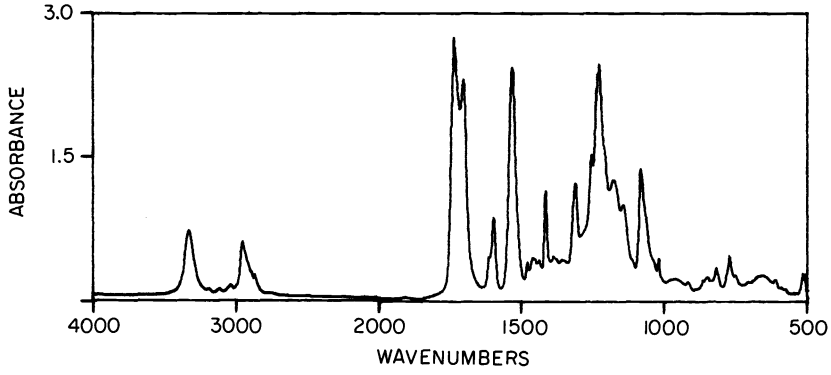

Fig. 14 IR spectrum of polyester urethane (b).

ν(C=O)urethane (1703 cm^{-1}), and δ(NH) + ν(CN) (1531 cm^{-1}) absorption bands, respectively. The analysis of the ν(C=O) absorption region, however, is complicated by the overlap of the hydrogenbonded ester- and urethane-carbonyl absorptions. Owing to their almost uncoupled nature and separate frequency positions the extent of hard and soft segment orientation has been monitored in the present investigation by the ν(NH) (3331 cm^{-1}) and $\nu(CH_2)$ (2959 cm^{-1}) absorption bands, respectively. Under the assumption that the transition moment directions for both vibrations make an angle of 90° with the polymer chain axis the corresponding orientation functions are represented by Eq. 4b. In view of the hard segment crystal structure proposed by Blackwell et al. and Born et al. (refs. 32,33), however, the maximum value to be expected for the ν(NH) orientation function is about 0.65. Furthermore, it has to be kept in mind, that in the original samples the ν(NH) absorption band represents not only the hard segments but also the isolated urethane units dispersed in the soft segment matrix. According to the Flory-Schulz distribution these structural units cover approximately 8.6%, 2.3% and 1.3% of the total NH-functionalities for polyester : diisocyanate molar ratios of 1 : 3.4, 1 : 6.6 and 1 : 8.7, respectively (ref. 34). A more differentiated characterization of hard segment orientation becomes available by the application of an isotope exchange technique with D_2O (ref. 26). The technique is limited to polymers containing loosely bonded protons in NH- or OH-functional groups and its applicability to the characterization of molecular order in polyurethanes is based on the fact that urethane and urea groups residing in chain segments of different degree of order are differently exposed to isotopic substitution. Thus, the NH-protons of the isolated urethane groups and small, fibrillar hard segments will be readily substituted by deuterium whereas the NH-protons of the phase-separated hard segments will not be accessible to deuteration. The percentage Z of accessible NH-functionalities at any stage of deuteration can be determined from the relationship:

$$Z = [1 - (A_{NH}/A_{NH_i})] \cdot 100(\%) \qquad (5)$$

where A_{NH} is the absorbance of the ν(NH) absorption band and i refers to the undeuterated sample. The IR spectra taken in regular time intervals during deuteration of polyester urethane (a) are shown in Fig. 15. The progress of isotopic H-D substitution can radily be deri-

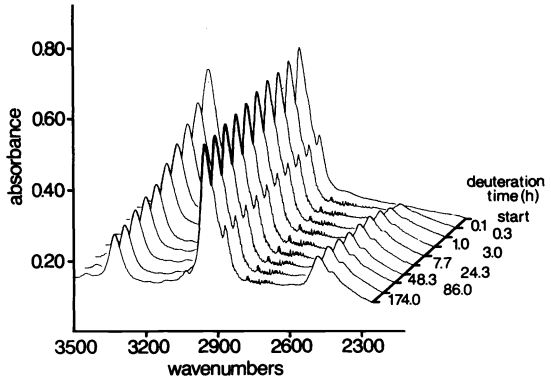

Fig. 15 IR spectra of polyester urethane (a) film in the 3500 - 2300 cm^{-1} wavenumber region taken in different time intervals during deuteration.

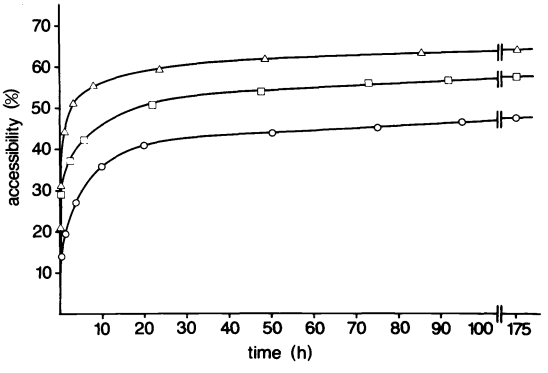

Fig. 16 Accessibilities to NH-ND substitution of the investigated polyester urethanes [(a): -△-, (b): -□-, (c): -○-] as a function of deuteration time.

ved from the intensity decrease and increase, respectively, of the ν(NH) (3331 cm^{-1}) and ν(ND) (2480 cm^{-1}) absorption bands. The corresponding accessibility/deuteration time-plots of the polyester urethanes (a), (b) and (c) are shown in Fig. 16 and roughly reflect the increasing proportion of isolated urethane units and small, primarily fibrillar hard segments relative to inaccessible, phase-separated segments with decreasing hard segment content.

The close relation between the composition and the mechanical properties of the polymers under examination is reflected by their stress-strain diagrams measured at 300 K (Fig. 17).

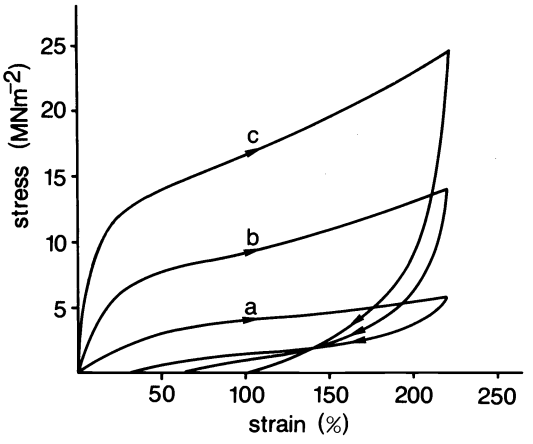

Fig. 17 Stress-strain curves of the loading-unloading cycles of the polyester urethanes with different hard and soft segment composition measured at 300 K.

Hence, for the specified experimental conditions a distinct increase of initial modulus (11, 45 and 120 MN/m^2), stress-hysteresis (60, 80 and 90%) and extension set (30, 65 and 100%) can be observed with increasing hard segment content of the polyester urethanes (a) to (c). The main consequences of temperature elevation to 348 K on the stress-strain diagrams are a general drastic decrease of stress level and the initial modulus and less significantly, an increase of extension set and stress hysteresis (ref. 26). The stress-strain diagrams of the partially NH-deuterated specimens did not substantially deviate from the mechanical data of the original polymers at ambient temperature and are also not shown separately.

Recently, Bonart (ref. 35) has shown that the extent of orientation of the hard segment phase during elongation depends on the morphology of the hard segment domains and the interrelationship of two deformation mechanisms based on a morphological and a molecular level. As long as the chains of the soft segments are randomly coiled the matrix can be regarded as a continuum and the hard segment domains will be oriented by a continuum mechanical transfer of stress with their long axis dimensions into the direction of stretch. Therefore, small, fibrillar hard segments in which the long axis dimension coincides with the polymer chain axes (Fig. 13

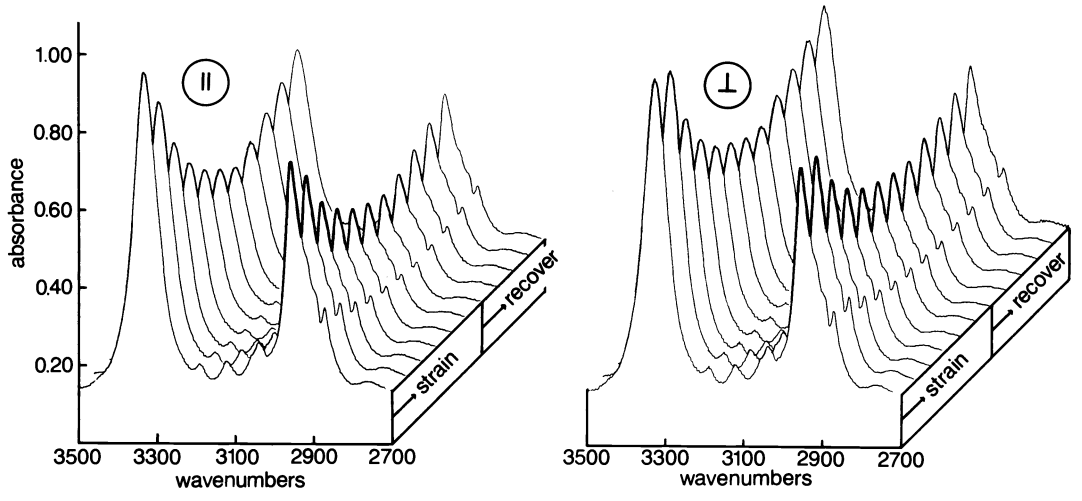

Fig. 18 FTIR polarization spectra of polyester urethane (c) in the ν(NH) and ν(CH_2) absorption region recorded at 300 K during uniaxial elongation to 220% strain and subsequent recovery to zero stress.

F) will take up a positive orientation while lamellar domains with their long axis dimension perpendicular to the polymer chain axes (Fig. 13 L) will be negatively oriented. This deformation mechanism dominates at low strains upto about 150% strain and the strain value of the maximum negative orientation depends on the stability of the lamellar morphology and the length of the soft segments. With increasing extension of the soft segments a molecular transfer of stress by individual chains becomes operative. For lamellar hard segment domains this mechanism leads to a disruption of the initially transversely oriented structural units with a subsequent positive orientation of the fragments into the direction of stretch. In the case of fibrillar hard segments continuum and molecular mechanical stress transfer both contribute to a positive alignment of the polymer chains.

To illustrate the dichroic effects the polarization spectra taken during elongation and recovery of polyester urethane (c) are shown separately for parallel and perpendicular polarization relative to the drawing direction in Fig. 18. The corresponding orientation functions of the ν(NH) and $\nu(CH_2)$ absorption bands have been plotted in dependence of strain for the three investigated polyester urethanes in Fig. 19. Thus, at ambient temperature upto the maximum elongation the soft segments exhibit a better average chain alignment in the direction of stretch than the hard segments. Additionally, the soft segments respond to the application of stress by an almost linear increase of positive chain orientation whereas an initial strain interval with orientation function values in the vicinity of zero is observed for the hard segments before the onset of significant positive orientation. This difference can be explained in terms of the abovementioned antagonism of lamellar hard segment alignment during elongation. In this region the positive orientation of small fibrillar hard segments is compensated by the negative orientation of lamellar hard segment domains and the shift in the onset of positive alignment to higher strain values for increasing soft segment content (polyester urethane (c) to (a)) is an indication for the corresponding increase in soft segment length. Upon recovery to zero stress the orientation is more effectively retained by the hard segments. This phenomenon may be attributed to the entropy-driven relaxation of the soft chain segments during unloading. As the soft segments relax they exert a tension on the hard segments thereby imposing an additional barrier to their recovery. The larger amount of residual orientation for increasing hard segment proportion is the result of a more extensive disruption of the hard segments during elongation. The orientation function/strain-plot derived from the polarization spectra monitored during the loading-unloading cycle of the polyester urethane with the largest hard segment content (c) at 348 K (Fig. 20) readily reflects the

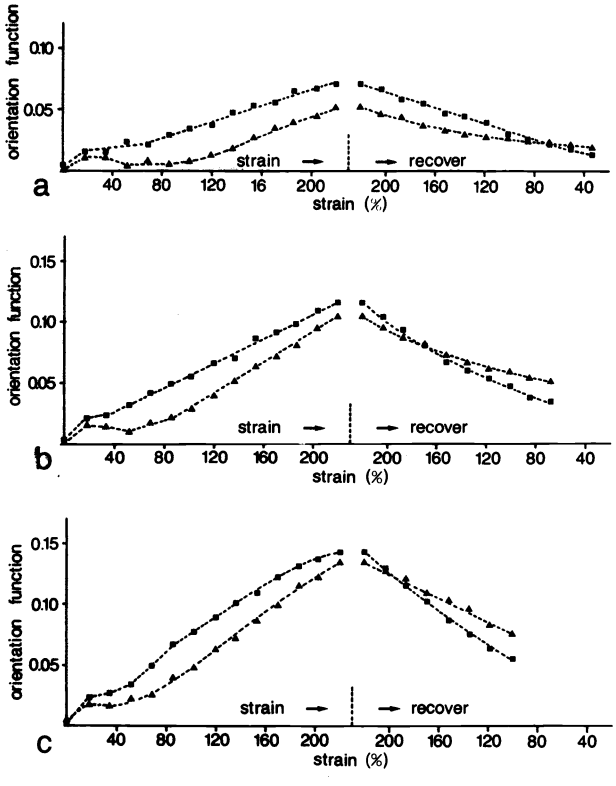

Fig. 19 Orientation function/strain-plot of the hard and soft segments of the polyester urethanes (a) to (c) as monitored by the ν(NH) (▲) and $\nu(CH_2)$ (■) absorption bands, respectively, at 300 K.

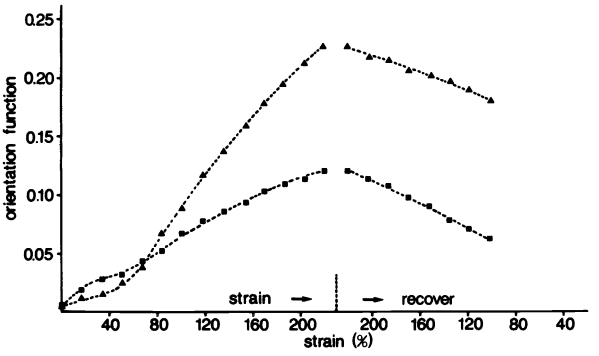

Fig. 20 Orientation function/strain-plot of the hard and soft segments of the polyester urethane (c) as monitored by the ν(NH)(▲) and ν(CH_2) (■) absorption bands, respectively, at 348 K.

main structural consequences of the mechanical treatment at elevated relative to ambient temperature:

a) earlier onset of positive hard segment orientation
b) drastic enhancement of hard segment orientation
c) slight deterioration of soft segment orientation
d) substantially larger retention of hard segment alignment upon recovery to zero stress.

These effects can be predominantly attributed to the temperature dependence of the domain structure in the polymers under examination. Thus, apart from a decrease of the degree of domain formation (ref. 36) the observed weakening of hydrogen bonding at elevated temperature (ref. 26) will also contribute to an increased disruption tendency of the hard segments upon application of stress. To demonstrate the possibility of differentiating the individual contributions to the average hard segment orientation the orientation function/strain-plot of the partially NH-deuterated polyester urethane (b) is shown in Fig. 21. Here, the ν(NH)

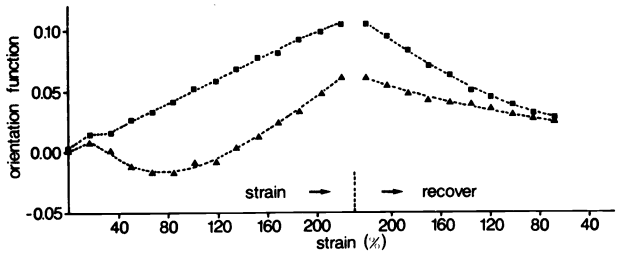

Fig. 21 Orientation function/strain-plot of the partially NH-deuterated polyester urethane (b) as monitored by the ν(NH)(▲) and ν(CH_2) (■) absorption bands, respectively, at 300 K.

orientation function represents the orientation of the inaccessible hard segments and according to Bonart's model of segmental orientation the pronounced transverse hard segment orientation is therefore consistent with the assignment of the involved urethane groups to phase-separated, lamellar domains. As can be readily derived from Fig. 21 the negative orientation of the hard segments does not immediately start with the application of stress. This supports a structural model proposed by Cooper (ref. 37) in which the hard segment domains are partly interconnected. Thus, the interconnections of such a hard segment network have to break up first before any transverse alignment can take place.

In conclusion, rheo-optical FTIR studies of this class of polymers provide a more detailed insight into phase separation and segmental orientation and recovery mechanisms and contribute towards a better correlation and optimization of their chemical structure and engineering applications.

ACKNOWLEDGEMENTS

The author gratefully acknowledges helpful discussions with Dr. U. Eisele, Dr. H. Hespe and Dr. G. Spilgies and thanks Bayer AG for the permission to publish the experimental data.

REFERENCES

1. H. W. Siesler, Adv. Polym. Sci., 65, 1-77 (1984).
2. D. G. Le Grand and P. F. Erhardt, Trans. Soc. Rheol., 6, 301-315 (1962).
3. R. S. Stein, J. Polym. Sci. Part C, 15, 185-222 (1966).
4. S. Onogi and T. Asada, Progr. Polym. Sci. Jap., 2, 261-328 (1971).
5. R. Zbinden, Infrared Spectroscopy of High Polymers, Academic Press, New York (1964).
6. B. Jasse and J. L. Koenig, J. Macromol. Sci. Rev. Macromol. Chem., C17, 61-135 (1979).
7. H. W. Siesler and K. Holland-Moritz, Infrared and Raman Spectroscopy of Polymers, Marcel Dekker, New York (1980).
8. R. J. Samuels, Makromol. Chem. Suppl., 4, 241-270 (1981).
9. W. W. Doll and J. B. Lando, J. Macromol. Sci. Phys., B4, 889-896 (1970).
10. A. J. Lovinger, Developments in Crystalline Polymers, p 195-279, Applied Science Publ., London (1982).
11. K. Matsushige, K. Nagata, S. Imada and T. Takemura, Polymer, 21, 1391-1397 (1980).
12. U. Kofer, R. Hirte and P. Weigel, Acta Polymerica, 33, 486-489 (1982).
13. B. A. Newman and J. I. Scheinbeim, Macromolecules, 16, 60-68 (1983).
14. M. Kobayashi, K. Tashiro and H. Tadokoro, Macromolecules, 8, 158-171 (1975).
15. M. A. Bachmann and J. L. Koenig, J. Chem. Phys., 74, 5896-5910) (1981).
16. H. W. Siesler, J. Polym. Sci. Polym. Phys. Ed., in press (1985).
17. P. J. Flory, Principles of Polymer Chemistry, Cornell University Press, New York (1953).
18. L. R. G. Treloar, The Physics of Rubber Elasticity, 3rd ed., Clarendon Press, Oxford (1975).
19. Y. Shimomura, J. L. White and J. E. Spruiell, J. Appl. Polym. Sci., 27, 3553-3567 (1982).
20. F. de Candia, G. Romano, R. Russo and V. Vittoria, J. Polym. Sci. Polym. Phys. Ed., 20, 1525-1531 (1982).
21. U. Eisele, Progr. Colloid & Polym. Sci., 66, 59-72 (1979).
22. J. E. Mark, Polym. Eng. Sci., 19, 254-259, 409-413 (1979).
23. M. Hashiyama, R. Gaylord and R. S. Stein, Makromol. Chem. Suppl., 1, 579-597 (1975).
24. H. W. Siesler, Colloid & Polym. Sci., 262, 223-229 (1984).
25. J. L. Binder, J. Polym. Sci. Part A, 1, 37-46 (1963).
26. H. W. Siesler, Polymer Bulletin, 9, 382-389, 471-478, 557-562 (1983).
27. H. Ishihara, I. Kimura, K. Saito and H. Ono, J. Macromol. Sci. Phys., B10, 591-618 (1974).
28. R. J. Bonart, L. Morbitzer and E. H. Müller, J. Macromol. Sci. Phys., B9, 447-461 (1974).
29. V. W. Srichatrapimuk and S. L. Cooper, J. Macromol. Sci. Phys., B15, 267-311 (1978).
30. I. D. Fridman and E. L. Thomas, Polymer, 21, 388-392 (1980).
31. Y. J. P. Chang and G. L. Wilkes, J. Polym. Sci. Polym. Phys. Ed., 13, 455-476 (1975).
32. J. Blackwell, M. R. Nagarajan and T. B. Hoitink, Polymer, 23, 950-956 (1982).
33. L. Born, H. Hespe, J. Crone and K. H. Wolf, Colloid & Polym. Sci., 260, 819-828 (1982).
34. R. Bonart and P. Demmer, Colloid & Polym. Sci., 260, 518-523 (1982).
35. R. Bonart and K. H. Hoffmann, Colloid & Polym. Sci., 260, 268-277 (1982).
36. G. L. Wilkes, S. Bagrodia, W. Humphries and R. Wildnauer, J. Polym. Sci. Polym. Lett. Ed., 13, 321-327 (1975).
37. J. W. C. Van Bogart, A. Lilaonitkul and S. L. Cooper, Adv. Chem., 176, 3-30 (1979).